Predicting iodine solubility at high pressure in borosilicate nuclear waste glasses using optical basicity: an experimental study

Yann MORIZET[a*], Michael PARIS[b], Jonathan HAMON[b], Carole LA[a], Stéphane GROLLEAU[b], Tomo SUZUKI-MURESAN[c]

[a]Nantes Université, Univ Angers, Le Mans Université, CNRS, UMR 6112, Laboratoire de Planétologie et Géosciences, F-44000 Nantes, France

[b]Nantes Université, CNRS, Institut des Matériaux de Nantes Jean Rouxel, IMN, F-44000 Nantes, France

[c]Nantes Université, IMT Atlantique, CNRS, SUBATECH, F-44000 Nantes, France

*Corresponding author: Yann Morizet

Postal address:

Laboratoire de Planétologie et Géodynamique (LPG), UMR-CNRS 6112, Université de Nantes.

2 rue de la Houssinière, 44322 Nantes Cedex (FRANCE)

phone: +33 (0) 2 5112 5491

fax: +33 (0) 2 5112 5268

*E-mail: yann.morizet@univ-nantes.fr

Abstract

Constraining the systematic evolution of iodine solubility in borosilicate glasses is required for the formulation of adequate glass matrices able to immobilize ^{129}I representing a major troublesome radioisotopes produced by nuclear anthropic activities.

We investigated experimentally the change in iodine solubility in a large series of borosilicate glasses synthesized under high-pressure conditions (1.5 GPa) and at 1350°C. The nature of network modifying cation (Na, K, Rb, Ca, Ba and Sr) and the concentration of B_2O_3 (~<10 mol.% and ~>10 mol.%) have been tested. The XPS measurements showed that iodine speciation in glasses is mostly represented by iodide (I^-) for a range of iodine solubility from 0.3 to 3.1 mol.% as determined by SEM EDS and LA-ICP-MS analyses.

The iodine solubility is enhanced in glasses with lower B_2O_3 content and with a higher concentration in network modifying cation. Regardless of the cation nature: alkali or alkaline-earth; increasing the cation size appears to induce a decrease in iodine solubility.

We used the optical basicity (Λ_{Glass}) and iono-covalent parameter (ICP_{Glass}) to express the large variety of investigated glass compositions; both relating to the electron donor capability of the glass. We show that iodine solubility is positively correlated to Λ_{Glass} and accordingly negatively correlated to ICP_{Glass}. It implies that more iodine will be dissolved in glass compositions having a stronger electron donating capability. Evidence of the relationship between iodine solubility and oxygen network is shown by the iodine solubility positive trend with equilibrium constant of the oxygen speciation. Future work should take these parameters into consideration for modeling iodine solubility in borosilicate glasses providing additional information are collected such as the boron, aluminum and silicon speciation in glasses.

Keywords: iodine solubility, optical basicity, high-pressure, nuclear waste

1. Introduction

In the many radioactive elements produced by anthropic nuclear sources, iodine (I) is one important volatile element representing a serious problem in the effort for the immobilization of radioactive wastes [1–5]. One particular isotope (^{129}I) requires a special attention because of 1) its long half-life (>15 Ma) and 2) its high mobility and volatility in environment [3, 6, 7]. Currently, several academic studies aim at developing durable conditioning matrices for this radioisotope but no ideal industrial solution has emerged for immobilizing it in a permanent and safe manner [8–17]. Although alternative surrogates have been recently suggested with phosphate glasses [18, 19], the immobilization of radioactive elements is often achieved in aluminoborosilicate glasses synthesized at ambient pressure, high-temperature and representing a good compromise that 1) will contain high concentration in radioactive elements to reduce the disposal space; 2) will be stable through time; 3) will not be damaged by radiation and heating; 4) will present high chemical durability [20–24]. However, owing to the high iodine volatility this protocol cannot retain efficiently ^{129}I radioisotopes that will escape from the melt to the atmosphere. Previous works [25–27] showed that the iodine solubility does not exceed 0.7 mol.% I in that case.

Recent investigations [28–30] demonstrate that the use of high-pressure synthesizing protocol of aluminoborosilicate glasses can circumvent this lack of iodine dissolution. For instance, Jolivet et al.[30] reached iodine solubility of 1.3 and 2.5 mol.% I in International Simple Glass (ISG, [31]) and typical Low Activity Waste glass (LAW, [32]) synthesized at 1.5 GPa, respectively. More recently, Morizet et al. [33] showed that the iodine solubility could be further increased by using highly oxidizing conditions promoting the formation of iodate species (I^{5+}) within the glass structure. Regardless, the strong increase in the iodine solubility is ascribed to the increase in thermodynamic activity of the fluidic iodine in equilibrium with the melt phase upon pressure [30, 34, 35]. Although, this represents a major breakthrough in

80 the race for immobilizing efficiently iodine radioisotopes, we still lack a clear fundamental
81 understanding on how iodine behave as a function of glass composition. At given intensive
82 conditions, the systematic evolution of iodine solubility as a function of glass composition is
83 currently poorly known.

84 Up to now, subsequent experimental investigations showed that iodine is sensitive to 1) the
85 presence of alkali cations in the glass [25–27, 36] and 2) the presence of boron (B_2O_3, [28–
86 30]). For simplified aluminoborosilicate glass compositions, McKeown et al. [27] and more
87 recently Morizet et al. [37] demonstrate that iodine dissolved as I^- is surrounded preferentially
88 by Na^+ cations for charge compensation, however, it appears that Ca^{2+} can also play this role
89 but to a lower extent. The formulation of a reliable nuclear waste glass matrix extends well-
90 beyond the case of Na and Ca. For example, the SON68 glass composition used in France for
91 immobilizing High Activity nuclear waste is composed of more than 25 different oxides [38].
92 The role of each element in glasses is fairly apprehended: either network former, or charge
93 compensating cation for network species with excess negative charges (e.g. AlO_4^-), or
94 network modifying cations. The latter category regroups number of element ranging from
95 alkalis (Na^+, K^+, Li^+, Rb^+), alkaline-earth (Ca^{2+}, Mg^{2+}, Ba^{2+}, Sr^{2+}), rare-earth elements (La^{3+},
96 Yb^{3+}), Bi^{3+} and others. These are supposed to be the elements that are mobilized for charge
97 compensating the I^- species as the charge compensating cation is tightly associated with the
98 network species having excess negative charges and there is no exchange between oxygen and
99 iodine atoms in network units [37]. As mentioned earlier the effect of Na^+ and Ca^{2+} on iodine
100 solubility is fairly understood; however, for the other elements we have virtually no
101 information.

102 As a result, there is a need for additional experimental investigations aiming at determining
103 systematically the change in iodine solubility as a function of glass composition in order to
104 propose the most adequate aluminoborosilicate glass formulation that can serve as a matrix

for the immobilization of ^{129}I radioisotopes. In the present work, we have investigated the change in iodine solubility as a function of glass composition involving different alkalis or alkaline-earth elements. Syntheses were done under high-pressure conditions with a I_2 fluid phase as a source of iodine; and, as expected, iodine speciation is represented by iodide species (I^-). The results are interpreted in terms of electrochemical parameters (optical basicity and iono-covalent parameter) that traduce the glass composition. We propose a discussion and some recommendations for future work to model iodine solubility and formulate an adequate aluminoborosilicate glass matrix for the immobilization of ^{129}I.

2. Experimental methods

2.1. Starting materials

Three series of aluminoborosilicate glass compositions were investigated in the present work. We cover a wide range of compositions having a common basis: SiO_2-Al_2O_3-B_2O_3; completed by various elements acting as network modifying or charge balancing cations: Na_2O, K_2O, Rb_2O, CaO, BaO and SrO. The first series consists in several glasses with a single network modifying cation either Na, K or Rb for alkalis or Ca, Ba, Sr for alkaline-earth elements. Within this group series, we prepared two different compositions: one with higher B_2O_3 content (B_2O_3 >10 mol.%) than the other (B_2O_3 <10 mol.%). The glass composition for this series with single network modifying cation is shown in the Table 1 for volatile-free glass synthesized at ambient pressure. The second glass series is composed of several Na-rich aluminoborosilicate glasses investigated in Jolivet et al. [39]: BASN3, BASN4, LJ4b (Al-free) and LJ8. Two additional compositions have been prepared, Na20Ca15B10Bi0-vf and Na30Ca10B10Bi0-vf, with the purpose of having an Iono-Covalent Parameter [40, 41] close to 1.00 and 0.96, respectively. These compositions have a mixture of CaO and Na_2O for the

network modifying or charge balancing cations. The third glass series corresponds to the first one in which a small amount of Bi_2O_3 (up to 4 mol.%) has been added.

The sample notation is the following: Ca20B20Bi0 that stands for the I-bearing pure Ca composition with higher B_2O_3 content and without Bi_2O_3; Ca30B10Bi3 stands for the I-bearing pure Ca composition with lower B_2O_3 content and with Bi_2O_3. The numbers in the sample name correspond to the targeted mol.% for each oxide. It should be noted that I-free glass synthesized at ambient pressure are reported in Table 1 and that the extension -vf is added to the sample name for simplicity; on the other hand, the I-bearing glass synthesized under high-pressure conditions are given in Table 2. For glass compositions from Jolivet et al. [39]: BASN3, BASN4, LJ4b (Al-free) and LJ8; we added the extension -vf and -I for I-free and I-bearing glasses in Table 1 and 2, respectively. Although, a potential industrial process is proscribed at pressure conditions of 1.5 GPa, this investigation has multiple objectives in the fundamental understanding of iodine behavior in aluminoborosilicate glass: 1) determine if iodine has higher affinity for one cation or another, 2) determine if the ratio between network modifier and network former cations impacts on the iodine solubility and 3) determine the influence of heavy Bi_2O_3 on iodine solubility.

The investigated glass compositions were prepared from a mixture of oxides (SiO_2, B_2O_3, Al_2O_3 and CaO) and carbonates (Na_2CO_3, Rb_2CO_3, $BaCO_3$ and $SrCO_3$). We used spec pure oxide and carbonate powders that were mixed under ethanol in an agate mortar. Prior to high-pressure experiments, the I-free starting material powders were melted at 1200°C in a Pt crucible. After 1h melting, the starting material is quenched to a glass by dropping the Pt crucible in a cold-water bath. Only one melting has been conducted in order to reduce the possible loss of alkali or boron oxides.

We loaded the sample powder into 2.9 mm outer diameter Pt capsule. The iodine was loaded as solid I_2 at the bottom of the capsule prior to add the glass powder. We prepared a mixture

154 with 0.01 g of I_2 and 0.04 g of glass powder that corresponds to ~10 mol.% I in the starting
155 composition. The Pt capsule is then welded shut using arc-welder at both ends. Our current
156 knowledge [30] indicates that the amount of loaded I_2 is sufficient to insure oversaturation
157 and I_2 should be in excess in the fluid phase during the experiments. For the Bi-bearing
158 sample series, the Bi-free glass powder was mixed with a small amount of Bi_2O_3 to reach 3 to
159 4 mol.% Bi_2O_3 in the collected I- Bi-bearing glass after the experiment.

160 2.2. High-pressure syntheses

161 The high-pressure I-bearing glasses were synthesized using end-load type piston-cylinder
162 apparatus (LPG Nantes). We used the same pressure and temperature conditions for all the
163 experiments: 1.5 GPa, 1350°C and for run duration of three hours insuring equilibrium to be
164 reached and comparison between the experimental results. The experiments were done using
165 ¾ inch talc-Pyrex assemblies and straight walls graphite furnace. Capsules are placed inside
166 Magnorite© ceramics preventing from a contact to the graphite furnace. Owing to the small
167 capsule diameter, two capsules are placed in the middle of the assembly; hence, both capsules
168 are experiencing the same intensive conditions (e.g. Na30Ca10B10Bi0 along with
169 Na20Ca15B10Bi0). The protocol to reach final pressure and temperature conditions is
170 described in previous works (e.g. [30, 42]): 1) increase in pressure to 1 GPa, 2) increase in
171 temperature to ~550°C for high-pressure assembly relaxation and compaction, 3) increase in
172 pressure to 1.5 GPa, and 4) increase in temperature to 1350°C. During the experiment, the
173 pressure is controlled automatically by a Stigma© needle pump; temperature is controlled by
174 a Eurotherm. The latter is accurate to ±1°C that is connected to a type B thermocouple ($PtRh_6$-
175 $PtRh_{30}$). Due to internal frictions, we applied a 10% correction to the pressure. Experiments
176 are stopped by cutting-off the power. The quench rate from 1350°C to room temperature is
177 ~100°C/s in the first 500°C. The quench is performed isobarically to prevent the formation of
178 bubbles that could distribute throughout the resulting glass.

179 The recovered samples consist in a colored (i.e. pink to brown) glass entirely coated with dark
180 coating that appears to be iodine residue. This residue implies that iodine in the fluid phase
181 was distributed throughout the experimental charge and it implies also that iodine was loaded
182 in excess prior to the experiment. We removed the excess iodine by dripping the glass pieces
183 into ethanol and then placing in a drying oven for a few minutes. Microscopic observation did
184 not reveal the presence of unwanted crystalline phases. It should be pointed out that several
185 experiments were replicated (e.g. Rb20B20Bi0-r is a replicate experiment of Rb20B20Bi0;
186 see Table 2) for insuring that measured I content is consistent, fully replicable, and not stained
187 by analytical bias.

188 2.3. Scanning Electron Microscopy with Energy Dispersive Spectrometer

189 We used Scanning Electron Microscopy with Energy Dispersive Spectrometer (SEM EDS) to
190 characterize the recovered glasses for major element and iodine concentrations. Glass chips
191 were mounted into epoxy resin plugs and subsequent polishing was done to 1 μm.
192 Measurements were conducted on a JEOL JSM 5800LV SEM (IMN Jean Rouxel), equipped
193 with a SDD SAMx dispersive spectrometer. The analytical conditions were 15 kV for voltage
194 and 0.5 nA for current. We conducted the acquisitions on a 20 μm spot size to avoid alkali (K,
195 Na and Rb) loss under the electron beam. Five scans of 1 min were collected on each sample
196 at different location on the glass chip.

197 We used the following internal standards for quantifying the elements: corundum for Al_2O_3,
198 wollastonite for SiO_2 and CaO, NaCl for Na_2O, BaF_2 for BaO, SrF_2 for SrO, KCl for K_2O,
199 RbI for Rb_2O and I, Bi metal for Bi_2O_3. We did not measure the B_2O_3 present in the
200 borosilicate glasses as it is not reliably quantified using SEM EDS due to the low boron
201 molecular mass. Based on the replicated measurements, we obtain an uncertainty on major
202 element measurements that is better than 5% in relative to the value and comparable to the
203 error reported in previous works on the same analytical equipment [30, 39]. For the particular

204 case of iodine, the typical error bar based on replicated measurement is ±0.2 mol.%. Data in
205 mol.% are provided in Table 1 for I-free glasses and in Table 2 for I-bearing glasses along
206 with the error that is calculated from the standard deviation of the replicated measurements.
207 The reported error pictures the homogeneity in the element distribution; however, we
208 observed slight heterogeneity in the major element concentrations for Ba30B10Bi0-vf
209 exhibiting larger error bars than for the other glasses.

210 2.4. Laser Ablation Inductively Coupled Plasma Mass Spectrometry

211 The B_2O_3 and I contents is determined using a Laser Ablation-Inductively Coupled Plasma-
212 Mass Spectrometry (LA-ICP-MS, LPG Nantes). The spectrometer is an ArF excimer laser
213 (193 nm, Analyte G2, Photon Machines) that is coupled to a quadrupole ICP-MS (Varian
214 Bruker 820-MS). The ablation is performed in a HelEx II 2-Volume Cell with He as carrier
215 gas. We used a laser energy density of 4.54 $J.cm^{-2}$ and with a repetition rate of 10 Hz. We
216 performed the acquisition in a spot mode with a diameter of 110 µm. We performed five
217 acquisitions on each I-bearing glass sample in static mode (i.e. point by point) on a glass
218 polished surface from the bulk and embedded into epoxy plug. The acquisition time was set to
219 30 s, preceded and followed by a 30 s blank acquisition. The washout time of the ablation cell
220 was approximately 50 s., due to the long residence time of iodine in the system. We estimated
221 the pit size to ~20 µm in depth that represents a large analyzed sample volume in comparison
222 to SEM EDS analyses. Only the LA-ICP-MS signal obtained slightly below the ablation
223 surface was considered for the quantification of iodine so as to avoid possible alteration in the
224 iodine content that could be generated from sample preparation[43].

225 LA-ICP-MS acquisition for I content is designed to corroborate the I results obtained by SEM
226 EDS. The data is calibrated against several glass samples. We recorded the ^{127}I and ^{27}Al
227 isotopes and this latter one was used as an internal standard. We calibrated the I content with
228 two high-pressure ISG glasses [31] doped with I (1.29 and 1.34 mol.% I) and with known

Al_2O_3 content of 4.08 and 4.02 mol.%, respectively. For these two samples, I and Al_2O_3 contents have been determined using Electron Probe Micro-Analyses (EPMA, ISTO Orléans) based on 400 points. We used the same protocol to quantify the B_2O_3 in glasses using LA-ICP-MS. For calibrating the B_2O_3 content in our glasses, we used the aluminoborosilicate glasses investigated by Jolivet et al. [39] that have been characterized using multiple techniques (SEM EDS, ^{11}B MAS NMR and ICP Optical Emission Spectrometry) for the quantification of B_2O_3. In particular, we used the LJ3, LJ4 and NH glasses from Jolivet et al. [39] having 34.9, 30.7 and 15.1 mol.% B_2O_3, respectively. The present calibration for I and B_2O_3 could not be used for I-bearing LJ4b glass sample as this glass does not contain Al_2O_3 currently used as the internal standard. For this sample, we considered the I content determined by SEM EDS and the B_2O_3 reported in Jolivet et al. [39]. We performed three analytical sessions on distinct glass chips for the Ca-bearing glass samples (Ca20B20Bi0 and Ca30B10Bi0) to check for consistency.

2.5. X-ray Photoelectron Spectroscopy

X-ray Photoelectron Spectroscopy (XPS) measurements were performed on each glass sample to determine the I and the O signatures in our glasses. XPS spectra for crystalline standards were not acquired considering that peak assignment has been previously reported for similar I-bearing glasses[33, 37, 44]. We carried out the XPS analyses on a Kratos Nova spectrometer (IMN Jean Rouxel) using a monochromatic Al Kα radiation operating at 1486.6 eV (15 kV, 20 mA). We analyzed glass chips (several mm^2) corresponding to a surface fracture from the bulk of the experimental charge. The surfaces were not prepared and the analyses were conducted on raw glass surfaces, hence avoiding possible surface contamination. The glass chips were loaded into the sample chamber under high-vacuum conditions ($<10^{-8}$ mbar). The spot size on the sample is 300x700 μm^2 area of analyses. We recorded survey spectra at a pass energy of 160 eV corresponding to an overall instrument resolution measured on silver Fermi

edge of 1.95 eV and a step of 0.5 eV from -5 to 1200 eV. High-resolution spectra of I 3d, O 1s, and C 1s core levels were recorded with an instrument resolution measured on silver Fermi of 0.49 eV and a step of 0.1 eV at a pass energy of 40 eV. We acquired the final spectrum with a cycling mode (several scan of the sample) for each element and we did not observe any modification of each individual acquisition that would suggest an alteration of the glass under the X-ray beam. We calibrated the XPS spectra using the adventitious C 1s in the binding energy at 284.8 eV. All spectra were treated with CasaXPS© software. We focused on the I $3d_{5/2}$ peak in the I 3d region, which exhibits the highest intensity as compared to the one for the I $3d_{3/2}$. The spectra were fitted with a U2 Tougaard function for the background [45]. Subsequent simulations are achieved with a pseudo-Voigt function with a Lorentzian ratio of 50% for the various peaks. The determination of the I species is accurate to within 10% of the derived value.

3. Results

3.1. Iodine speciation from XPS

For an adequate comparison, the samples have to exert the same or similar iodine speciation. Iodine exhibits several redox degree ranging from -1 to +7. During the high-pressure experiments, no constraints were placed on the redox conditions and the talc-Pyrex assembly fixes the fO_2 intrinsically. It has been previously estimated that talc-Pyrex assembly imposes fO_2 conditions relatively oxidizing at +1 log unit above the solid buffer QFM (QFM+1, Quartz-Fayalite-Magnetite, [46]). Even though the redox conditions are relatively oxidizing, we have previously shown that under those conditions iodine is mostly dissolved under its reduced iodide form: I^- [30, 33].

The XPS results in the I 3d region is shown in Figure 1. For clarity, we show the spectra obtained on the glasses with alkali and high B_2O_3 (Figure 1A) and with alkaline-earth and low B_2O_3 (Figure 1B) cations; the entire set of spectra is available in the Suppl. Mat.. In addition, the XPS spectra in the O 1s region (~532 eV) for the whole set of glasses were acquired. For clarity, the O 1s XPS are only provided in the Suppl. Mat.. The O 1s located at ~532 eV and is approximately symmetric. For the O 1s spectra, the peak maximum position has been determined as a function of glass composition. In Figure 1, we choose to represent only the I $3d_{5/2}$ region that represents the most intense iodine peak. The peak located at 619 eV corresponds to the signature of iodide (I^-) species as identified in previous works [33, 37, 44, 47, 48]. For several samples (see Suppl. Mat.), we have observed a slight asymmetry on the high-energy side (~621 eV) that could correspond to the presence of I^0 species [49]. Currently, I^0 has also been identified in previous studies for glasses [37, 44] and could correspond to micrometric bubbles of solid I_2 or effectively dissolved I_2 species within the glass. This aspect is not clarified yet. For K20B20Bi0, we observed an additional peak located at ~624 eV that we assigned to the presence of a slight amount of iodate species (I^{5+}, [33]). It is also observed for several additional samples: Na30B10Bi0, K30B10Bi0, BASN4-I, Na30Ca10B10Bi0 and Na20Ca15B10Bi0; and does not exceed 10% in relative to the iodine species. Nevertheless, the existence of the most oxidized iodine species is systematically observed in the most iodine rich samples. For instance, for K30B10Bi0 in which 1.9 mol.% I is measured by LA-ICP-MS, the proportion of I^{5+} is 9.9% whereas in Rb20B20Bi0 in which 0.3 mol.% I is measured, the I^{5+} is absent. However, the proportion of I^{5+} is low enough for samples to be compared to each other and in the present work; iodine is mostly dissolved as I^- species. The derived XI^- is reported along to the spectra and is determined from the spectrum simulation (values are provided in Table 1). As mentioned, this result is consistent with

previous work [33, 37] that suggested the following dissolution mechanism for iodine in aluminoborosilicate glasses:

$$\frac{n}{2} I_2^{melt/fluid} + M^{n+}..O_n^{-\,NBO} \leftrightarrow M^{n+}..I_n^{-} + \frac{n}{2} O_2^{fluid/melt} + \frac{n}{2} O^{BO} \qquad \text{Eq. 1}$$

In Eq. 1, the M^{n+}, O^{NBO} and O^{BO} stand for a charge compensating cation (e.g. alkali or alkaline-earth cations), a Non-Bridging Oxygen and a Bridging Oxygen from the glass structure, respectively. Interestingly, the chemical reaction implies that there is, at some point, an interaction between I_2 molecules in the fluid phase and the oxygen atoms of the melt. Moreover, the Eq. 1 also suggests that there is a transfer of negative charge from the oxygen to the iodine to form iodide species. The Eq. 1 points to the fact iodine dissolution is accompanied by an increase in the degree of polymerization as inferred in recent work [36].

3.2.Effect of network modifying cations on iodine solubility

The iodine solubility data obtained by LA-ICP-MS and SEM EDS are provided in Table 1. Both acquisitions compare adequately suggesting that acquired iodine solubility data are robust. As mentioned earlier, the error (in bracket) represents the homogeneity of the iodine distribution within the sample (i.e. standard deviation obtained on multiple analyses).. For SEM EDS measurements, the analytical error is on the order of ±0.2 mol.% similar to the error reported in Jolivet et al. [30]. The analytical error associated with LA-ICP-MS is suspected to be lower (±0.1 mol.%) and more representative of the glass iodine content. The volume analyzed by LA-ICP-MS spot is larger (spot of 110 µm in diameter by 20 µm in depth) than the surface analyzed by SEM EDS (~20 μm^2). For the remaining of the manuscript, we will preferentially consider the data obtained by LA-ICP-MS unless those are not available.

The change in iodine solubility as a function of the network modifying cation is represented in Figure 2, for glass compositions with B_2O_3>10 mol.% and with B_2O_3<10 mol.%. In Figure 2, the glass compositions have been categorized in term of increasing cation charge (alkali before alkaline-earth) and increasing cation size ($Na^+ \rightarrow K^+ \rightarrow Rb^+$ and $Ca^{2+} \rightarrow Sr^{2+} \rightarrow Ba^{2+}$).

At B_2O_3<10 mol.%, we observe that iodine solubility seems to be higher in alkali-bearing glasses than in alkaline-earth bearing glasses. In detail, the iodine solubility is higher for Na-bearing glass than for Ca- and Sr-bearing glasses. We observe that iodine solubility for K- Ca- and Sr-bearing glasses are roughly the same. Previous investigations [27, 30, 33] suggested that iodine dissolved as I^- species has a better affinity towards alkali atoms rather than alkaline-earth atoms. Our results are consistent with that statement at least for Na-bearing glass in comparison to alkaline-earth ones. However, at B_2O_3>10 mol.%, the evolution of the iodine solubility depending on the network modifying cation nature is much more complex. There is a clear decrease in the iodine solubility with increasing cation size within each category: alkali, I solubility decreases from Na to Rb; alkaline-earth, I solubility decreases from Ca to Ba. We observe a non-monotonic change in iodine solubility with a jump in iodine solubility between Rb and Ca glass compositions. Unexpectedly, the iodine solubility appears higher in alkaline-earth bearing glasses than in alkali-bearing glasses at B_2O_3 concentration above 10 mol.%.

4. Discussion

4.1. Electrochemical parameters for aluminoborosilicate glass compositions and the relationship to oxygen activity

In the present study, the range of investigated glass compositions is relatively large: different boron contents, different network modifying cations, and mixing between network modifying cations; therefore explaining the change in the iodine solubility requires expressing the studied glass compositions with chemically relevant bulk parameters. To do so, we have

focused our approach on the pioneer work by Duffy [50, 51] that defined an oxide glass by its optical basicity (Λ). The optical basicity takes its origin into the Lewis acidity concept. The optical basicity also relates to the Jørgensen's nephelauxetic parametrization that corresponds to the electron donation to cations and the resulting degree of charge reduction experienced by these ions [52, 53]. The optical basicity has been applied for describing many properties such as the refractive index, the UV transparency, the redox behavior of glass melts, and the viscosity dependence with temperature [54]. In the present work, we have calculated the glass optical basicity (Λ_{Glass}) according to the equation of Duffy [50]:

$$\Lambda_{Glass} = \sum \frac{X_i}{\gamma_i} = \sum X_i \times \Lambda_i \qquad \text{Eq. 3}$$

In which X_i represents the molar fraction of the oxide i and γ_i corresponds to the basicity moderating parameters of the oxides. For the investigated glasses, we used the γ_i or Λ_i ($1/\gamma_i$) for SiO_2, Al_2O_3, B_2O_3, CaO, SrO, BaO, Na_2O, K_2O, Rb_2O and Bi_2O_3 reported in previous works (e.g. compilation of γ_i values in Rodriguez et al. [55]). The calculated Λ_{Glass} is reported in Table 1 for volatile-free glasses and in Table 2 for I-bearing glasses. It should be pointed out that the calculated Λ_{Glass} represents a theoretical value as the true optical basicity value (Λ_n) can only be obtained via the glass refractive index (n) measurement [56–58]. Because of the small glass sample size, we could not measure the optical refractive index.

The second glass bulk parameter considered here has been defined by Portier et al. [40, 41] and corresponds to the Iono-Covalent Parameter (ICP). The ICP is related to the acidic strength and takes into account the ionic-covalent character of a bond. In other words, the ICP takes into account the ionic forces (polarizing power) and the covalent forces (electronegativity). This aspect is particularly designed for glasses having both covalent and ionic characters. Furthermore, providing that iodine is dissolved as I^- species it has a ionic character and I^- is surrounded by network modifying cation (Na^+ or Ca^{2+}, [37]), it is likely that

a relationship between ICP and iodine solubility exists. The ICP_i parameter for each oxide is calculated with the following equation from Portier et al. [40, 41]:

$$ICP_i = log\left(\frac{z_i}{r_i^2}\right) - 0.6\chi_{i(a-r)} + 1.21 \qquad \text{Eq. 3}$$

Where z_i/r_i^2 corresponds to the polarizing power of cation i and $\chi_{i(a\text{-}r)}$ is the cation electronegativity as defined by Allred and Rochow [59]. The ICP for the glass is then determined as follow:

$$ICP_{Glass} = \sum X_i ICP_i \qquad \text{Eq. 4}$$

Where X_i is the molar fraction of the cation in the glass composition. The values for ICP_{Glass} are provided in Table 1 and Table 2. The calculation of ΛGlass and ICPGlass are provided in Suppl. Mat..

The data points are shown in Figure 3 and the ICP_{Glass} is reported as a function of Λ_{Glass} only for the volatile-free glasses obtained at ambient pressure. In the present calculations, several aspects related to structural information are not taken into account in the calculation of Λ_{Glass}. Recent works [53, 60] indicate that the theoretical optical basicity values will be better approached if we take into account 1) the distribution of BO_4 and BO_3 within the glass (i.e. N_4 and N_3 values, [20, 39, 61, 62]), 2) the distribution of silicate network Q^n species [63–66], and the distribution in the aluminum species (i.e. 4-, 5- and 6-coordinated species, [67–69]. In the present work, we do not have access to this information, as it would involve advanced NMR acquisition. Furthermore, our glass samples are prepared under high-pressure conditions and the effect of this intensive parameter on the optical basicity and iono-covalent parameter defined by Duffy [50] and Portier et al. [40, 41] is currently not constrained but should exist. For instance, Kuryaeva [70] shows that increasing pressure induces an increase in the glass refractive index. The increase in the refractive index increases the oxide ion polarizability [56,

57, 71] and hence changes the optical basicity value [51, 57, 71]. In the Suppl. Mat. we provide the same figure as Figure 3 but completed with the I-bearing data provided in Table 2. The reason for which we do not include those points in the actual Figure 3 is because the effect of pressure and iodine on the ICP_{Glass} and Λ_{Glass} is currently unknown.

Nevertheless, in Figure 3, we clearly see that there is a negative correlation between ICP_{Glass} and Λ_{Glass}. This relationship is expected and has been shown in previous works [72, 73]: Λ is the numerical expression of the average electron donor power of the oxide species and ICP represents the influence of ionic-covalent bonding in an oxide on the acid strength of the cations. Furthermore, Reddy et al. [74] demonstrated that Λ correlates linearly with the average electronegativity. Hence, both parameters (ICP_{Glass} and Λ_{Glass}) are correlated to each other; however, the method to calculate each parameter is different. Λ is strongly dependent on the cation polarizing power: in ionic solids (i.e. cations have weak polarizing power), the charges are focused on each ion and the oxygen will be able to give an important partial negative charge to a new cation; in solids with important covalent character in the chemical bonds, the negative charge will be shared by the cation and the anion and the oxygen will have a weak electron-donating power. In the present dataset, the extremes of the trend define two different glass behaviours: one more acidic at lower Λ_{Glass} and higher ICP_{Glass}, one more basic at higher Λ_{Glass} and lower ICP_{Glass}. The latter case implies higher electronegativity global value and a higher electron donation capacity from the oxygen atoms. From Figure 3, the two investigated parameters can be used to express the bulk chemical properties of the glasses. In the investigated glasses, the alkaline-earth-bearing glasses have the highest ICP_{Glass} values and the lowest Λ_{Glass}. On the contrary, the alkali-bearing glasses have the lowest ICP_{Glass} and the highest Λ_{Glass}. For glasses with a mixture of CaO and Na_2O, the ICP_{Glass} and the Λ_{Glass} values are located in the region of the alkali-bearing data point, which could be explained by the higher concentration of Na_2O in comparison to CaO (see Table 1).

In the present work the glass optical basicity can only be accessed through calculation; however, it has been shown that Λ_{Glass} is negatively correlated to the change in O 1s peak maximum measured by XPS considering that the Λ_{Glass} represents the measure of the valence charge density surrounding the oxygen ion in the network [56, 75, 76]. The change in the Λ_{Glass} for volatile-free glasses as a function of the O 1s peak maximum is shown in Figure 4. The same figure is proposed in the Suppl. Mat. and includes the data for I-bearing glasses. The correlation observed in Figure 4 witnesses that the optical basicity relates intimately to the oxygen activity within the glass [77]. It also shows that the positioning of the optical basicity numerical value is correct from one glass composition compared to another even though the glass structure is only partially known.

4.2. I solubility prediction using glass optical basicity and iono-covalent parameter

The prime objective of this work is to investigate the change of iodine solubility as a function of glass composition that can be expressed by different bulk chemical parameters. We show the change in iodine solubility (in mol.% I) as a function of Λ_{Glass} and ICP_{Glass} in Figure 5A and 5B, respectively. In Figure 5, we added the data points from Jolivet et al. [30] acquired at identical pressure (1.5 GPa) and for two different glass compositions: ISG and NH. The recent I solubility data points from Morizet et al. [33] are also added. These data were obtained on Ca- and Na-bearing aluminoborosilicate glasses synthesized at pressure conditions of 1.5 GPa.

The data from Jolivet et al. [30] and most of the data from Morizet et al. [33] compare adequately with our data in Figure 5. One data point (Λ_{Glass} = 0.747 and 3.9 mol.% I) from Morizet et al. [33] seems to be off the general trend. Actually, one possible explanation is the presence of a substantial quantity of I^{5+} in this glass sample that has not been accounted for and would explain the high I solubility for instance for their C0N35 at 3.9 mol.% I. Although, there is a significant scatter in the data, which we believe, is resulting from an inadequate

approximation in the Λ_{Glass} and ICP_{Glass} as mentioned earlier; we observe a reasonable correlation between iodine solubility and Λ_{Glass} and ICP_{Glass}. There is a positive correlation of iodine solubility with increasing Λ_{Glass} and a negative correlation with ICP_{Glass}, which is consistent with the observed correlation between Λ_{Glass} and ICP_{Glass} shown in Figure 3.

The results shown in Figure 5 suggest that iodine solubility in aluminoborosilicate glasses can be derived providing the optical basicity or the iono-covalent parameter are known, however, a better accuracy is requested in the calculation of these compositional parameters. As mentioned earlier, knowledge on the distribution of boron species (i.e. N_4 and N_3) is required for calculating a more accurate value for Λ_{Glass}. In Figure 5A, the NH23-1 from Jolivet et al. [26] has been fully characterized in Jolivet et al. [26] that report a N_4 value at 0.45 with iodine content at 1.9 mol.%. The iodine speciation for this sample is provided in Morizet et al. [33] and is 100% I^-. With the current simple calculation for the glass optical basicity: all B_2O_3 is in trigonal boron unit (BO_3) configuration and considering $\gamma_{BO3} = 2.47$ [78]; we obtain a Λ_{Glass}(NH23-1) = 0.730. Taking into account the distribution of B_2O_3 as 55% BO_3 and 45% BO_4 ($N_4 = 0.45$ reported in Jolivet et al. [26]) and $\gamma_{BO4} = 4.17$ [60], we calculate a Λ_{Glass}(NH23-1) = 0.707. Such a change represents a variation of ~2% in relative to the value. We report the difference in Λ_{Glass}(NH23-1) in Figure 5A. Unfortunately, it appears impossible to apply systematically this Λ_{Glass} variation to all the data points as the change in N_4 value is a complex function of the glass composition and the optical basicity variation in the studied glasses is not necessarily identical to the one calculated for NH23-1.

Previous works [26] suggest that N_4 value is likely to influence the iodine solubility. Currently, the model from Lu et al. [79] determines the N_4 for a large range of glass composition; however, this model is not designed to be applied for high-pressure glasses. There is a gap in our understanding of the effect of pressure on the distribution of boron species in glasses. Previous investigations [80–82] demonstrate that increasing pressure

provokes an increase in the N_4 value. Nevertheless, Jolivet et al. [26] showed that the change in N_4 value upon pressure increase is probably dependent on the glass composition. Furthermore, it is not clear if the iodine dissolution itself have or not an effect on the N_4 value.

In a similar manner, the distribution in the silicate network units (i.e. Q^n species where n represents the number of bridging oxygen) should be determined for calculating an accurate Λ_{Glass} as suggested by Dimitrov et al. [60]. From another viewpoint, the distribution of Q^n species describes the degree of polymerization of the glass, namely, the connectivity between silicate network units. The higher the SiO_2, higher is the degree of polymerization and silicate network units have higher connectivity.

In the present work, the use of bismuth oxide could appear odd, however, we justify the addition of Bi_2O_3 to the studied glass compositions by two aspects: 1) Bi_2O_3 is often used in nuclear waste glasses for its good radiation shielding ability and 2) with its low γ value, Bi_2O_3 could be a good oxide candidate that increases the Λ_{Glass} and hence we expect an increase in I solubility with the addition of Bi_2O_3. These two aspects are further discussed below.

First of all, bismuth (present as Bi^{3+}) is recognized to present good shielding capacity to irradiation [83], hence representing a pertinent oxide to add in the borosilicate glass matrix for the immobilization of nuclear waste. Moreover, recent works demonstrate that bismuth is gaining great interest in glass technology, in particular in optics and photonic (e.g. [84–87]). As mentioned earlier, the role of bismuth in glasses is similar to the one of alkali (or alkaline-earth) elements. It acts as a network modifying cation inducing a depolymerization of the glass structure and high concentration of NBOs in the surrounding of Bi^{3+} ions. It is recognized that these two aspects have a positive effect on the higher dissolution of iodine[30, 33, 36]. In Figure 5A, adding a small quantity of Bi_2O_3 seems to induce an increase in the I solubility for alkali-bearing glasses. For alkaline-earth-bearing glasses, we observe that

adding Bi_2O_3 to Ca-bearing glasses has an opposite effect and I solubility is decreasing. This aspect is currently not explained and needs further investigations.

Second of all, in term of optical basicity, Bi_2O_3 has a low moderating parameter (γ_{Bi2O3} = 0.84; [84]) that induces an increase in Λ_{Glass} and an increase in iodine solubility is expected. Hence, the small addition of element having low moderating parameters such as Cs_2O with γ_{Cs2O} = 0.60 [51] would be beneficial for dissolving higher concentration of iodine in glasses. This aspect remains to be confirmed. For instance, the Rb-bearing glass composition (Rb20B20Bi0-vf) for which Rb_2O has a low moderating parameter (γ_{Rb2O} = 0.67, [53]), on the contrary, does not exhibit a high iodine concentration: 0.3 mol.% I in Rb20B20Bi0. Further experimental work is currently required to address in more details the change in iodine solubility in presence of heavy elements such as bismuth.

4.3. Iodine solubility and dissolution mechanism and its relationship to the glass degree of polymerization

It has been shown that a borosilicate melt could be described by a speciation model made of several equilibrium reactions. In particular, several types of oxygen species coexist within the melt with the following equilibrium reaction to describe it [77, 88–90]:

$$2O^{-\,NBO} \overset{K_{Oxygen}}{\longleftrightarrow} O^{0\,BO} + O^{2-free} \qquad \text{Eq. 5}$$

Where $O^{-\,NBO}$ represents the Non-Bridging Oxygen, $O^{0\,BO}$ represents the Bridging Oxygen and $O^{2-\,free}$ is a free oxygen species that could be linked to available cations such as alkalis, alkaline-earth cations or bismuth. In other words, Eq. 5 represents the degree of polymerization of the melt as seen from the anionic oxygen species viewpoint. From Eq. 5, the equilibrium constant can be written as follow:

$$K_{Oxygen} = \frac{a_{O0\,BO}^{Melt} \times a_{O2-free}^{Melt}}{\left(a_{O-NBO}^{Melt}\right)^2} \qquad \text{Eq. 6}$$

519 Where a_i^{Melt} corresponds to the thermodynamic activity of the i species in the melt; that is
520 related to the actual concentration of the i species from standard thermodynamic relationship
521 such $a_i^j = X_i^j \Gamma_i^j$; where X_i^j and Γ_i^j are the molar fraction and the activity coefficient of the i
522 species, respectively. Since we do not have access to a measure of the actual molar fraction of
523 the different oxygen species, the K_{Oxygen} cannot be solved directly; nevertheless, Moretti [77]
524 mentioned that the K_{Oxygen} is related to the optical basicity by the following equation:

525 $$K_{Oxygen} = \exp[4.662 \times (\sum X_{M^{m+}} \gamma_{M^{m+}} - \sum X_{T^{t+}} \gamma_{T^{t+}}) - 1.1445] \quad \text{Eq. 7}$$

526 In Eq. 7, the K_{Oxygen} is a function of the molar fraction (X_i) and the optical moderating
527 parameter (γ_i). The K_{Oxygen} is calculated with the difference between the network forming
528 (T^{t+}) and the network modifying cations (M^{m+}). Although Moretti [77] used this approach to
529 silicate melts and glasses, we believe that the same can apply to the present study for
530 aluminoborosilicate glasses.

531 In the present work, the network forming cations are Si^{4+}, Al^{3+} and B^{3+} whereas the network
532 modifying cations are Na^+, K^+, Rb^+, Ca^{2+}, Sr^{2+}, Ba^{2+} and Bi^{3+}. The calculated values for
533 K_{Oxygen} are provided in Table 2 and we plotted the change in iodine solubility in mol.% as a
534 function of the K_{Oxygen} value in Figure 6. For the whole investigated series, there is a clear
535 increase in the mol.% I with the increase in the K_{Oxygen} value. Three series (the mixed alkali
536 and alkaline-earth, the alkali without Bi_2O_3 and the alkali with Bi_2O_3) have been fitted with an
537 exponential growth function as a guide for the reader. The K_{Oxygen} values for the alkaline-earth
538 series did not allow to fit reasonably the data.

539 Considering that the K_{Oxygen} is calculated regardless of the iodine content, the observed
540 increase in Figure 6 is related to the distribution of oxygen species concentrations. In the
541 present work we have shown that iodine is dissolved as I^- species and from previous works
542 [30, 33] it has been shown that the dissolution mechanism follows the Eq. 1 chemical reaction

in which I^- is charge compensated by alkali or alkaline-earth cations. From the results in Figure 6, we suggest that iodine dissolution could be related to the presence of free oxygen within the glass structure (and by extension to the presence of network modifying cations). According to the proposed model, the more free oxygen is present the more iodine can be dissolved as I^-. Hence, the iodine dissolution reaction proposed with Eq. 1 could also be rewritten by considering the presence of free oxygen such as:

$$I_2^{fluid} + O^{2-free} .. \frac{2}{m} M^{m+free} \rightarrow 2I^- .. \frac{2}{m} M^{m+} + {}^1/_2\, O_2^{fluid} \qquad \text{Eq. 8}$$

In Eq. 8, the formation of iodide is promoted by the fact that iodine thermodynamic activity in the fluid phase is high owing to the excess iodine loaded during the experiment. Regardless of the glass compositional effect, the iodine solubility is proportional to the iodine fugacity imposed by the experimental pressure and temperature conditions: $[I^-] \propto f_{I_2}^{fluid}$. On the contrary at ambient pressure the iodine fugacity is close to 1 and the iodine solubility is low [25, 27, 36]. At high optical basicity (i.e. high K_{Oxygen} value), the high free oxygen concentration facilitates the formation of iodate species (IO_3^-), which means that free oxygen species are not entirely exsolved in the fluid phase.

In the mechanism proposed in Eq. 8, there is no apparent change in the degree of polymerization of the glass, however, because free oxygen is exsolved in the fluid phase upon iodine dissolution, there should be a re-equilibration in the distribution of NBO and BO concentrations. This contrasts with the recent proposition by Morizet et al. [33] in which the involved oxygen species in the iodine dissolution are NBOs that are transformed into BOs inducing an increase in the degree of polymerization of the glass. Currently, in the absence of strong advanced NMR investigations (i.e. ^{17}O NMR) we can only propose reasonable hypotheses for type of oxygen species involved in the dissolution of iodine. Nevertheless, the

iodine dissolution has necessarily an impact on the glass structure with a change in the distribution of oxygen species.

5. Summary

In the present work, we have synthesized a large series of aluminoborosilicate glasses under high-pressure conditions (1.5 GPa) in equilibrium with a iodine fluid phase. With the different syntheses, we have tested 1) the effect of various network modifying cation (Na, K, Rb, Ca, Sr and Ba), 2) the effect of boron concentration with either <10 mol.% or >10 mol.% B_2O_3 and 3) the effect of the addition of a small quantity of Bi_2O_3 (~4 mol.%).

We have shown that there is a complex change in iodine solubility with the nature of glass containing cations but also dependent on the B_2O_3 concentration: at high B_2O_3, iodine solubility increases with the following suite of cation: Rb < Ba = K < Na < Ca; at low B_2O_3, iodine solubility increases with the following suite of cation: Ba < Sr < Ca = K < Na. Increasing the B_2O_3 concentration in the glass (i.e. decreasing the network modifying cation concentration) does not favor the iodine dissolution and solubility decreases. Apart for Ca-bearing glasses, the addition of Bi_2O_3 induces an increase in iodine solubility that we ascribe to the structural role of Bi atoms comparable to the network modifying cation.

We have shown that iodine solubility is correlated positively with the optical basicity (Λ_{Glass}) and negatively correlated to the Iono-Covalent Parameter (ICP_{Glass}). This is consistent with the fact that Λ_{Glass} reflects the electron donor capacity of oxygen and that there is a transfer of negative charge to dissolve iodine as I^- species. As a result, both ICP_{Glass} and Λ_{Glass} could serve as predicting parameters for formulating a glass matrix able to immobilize a large quantity of ^{129}I. The most adequate glass composition should exhibit a high optical basicity;

however, there is a compromise to find as increasing the glass optical basicity would reduce the glass chemical durability.

Acknowledgement

The authors are grateful to the Agence Nationale de la Recherche and Région Pays de la Loire, which financed the current work through the ANR project "Iodine-CLEAN-UP" (ANR-20-CE08-0018) and the Pari Scientifique "CIPress". The authors thank the Laboratoire de Planétologie et Géosciences, the Institut des Matériaux de Nantes Jean Rouxel, Nantes Université and the CNRS for providing access to the analytical facilities. The authors thank Nicolas Stephant for its support on the SEM/EDS analytical platform. We would like to thank Ida Di Carlo (ISTO) for providing the EPMA analyses.

Compliance with Ethical Standards:

Funding: This study was funded by Agence Nationale de la Recherche through the project "Iodine-CLEAN-UP" (ANR-20-CE08-0018) and the Région Pays de la Loire through the Pari Scientifique "CIPress X".

Conflict of Interest: The authors declare that they have no conflict of interest.

References

1. Aldahan A, Alfimov V, Possnert G (2007) ^{129}I anthropogenic budget: Major sources and sinks. Applied Geochemistry 22:606–618. https://doi.org/10.1016/j.apgeochem.2006.12.006

2. Michel R, Daraoui A, Gorny M, et al (2012) Iodine-129 and iodine-127 in European seawaters and in precipitation from Northern Germany. Science of The Total Environment 419:151–169. https://doi.org/10.1016/j.scitotenv.2012.01.009

3. Chen X, Gong M, Yi P, et al (2015) Distribution of ^{129}I in terrestrial surface water environments. Nuclear Instruments and Methods in Physics Research Section B: Beam Interactions with Materials and Atoms 361:604–608. https://doi.org/10.1016/j.nimb.2015.04.073

4. Hu Q, Zhao P, Moran JE, Seaman JC (2005) Sorption and transport of iodine species in sediments from the Savannah River and Hanford Sites. Journal of Contaminant Hydrology 78:185–205. https://doi.org/10.1016/j.jconhyd.2005.05.007

5. Reithmeier H, Lazarev V, Rühm W, Nolte E (2010) Anthropogenic ^{129}I in the atmosphere: Overview over major sources, transport processes and deposition pattern. Science of The Total Environment 408:5052–5064. https://doi.org/10.1016/j.scitotenv.2010.07.015

6. Englund E, Aldahan A, Hou XL, et al (2010) Iodine (^{129}I and ^{127}I) in aerosols from northern Europe. Nuclear Instruments and Methods in Physics Research Section B: Beam Interactions with Materials and Atoms 268:1139–1141. https://doi.org/10.1016/j.nimb.2009.10.118

7. Fan Y, Hou X, Zhou W, Liu G (2016) ^{129}I record of nuclear activities in marine sediment core from Jiaozhou Bay in China. Journal of Environmental Radioactivity 154:15–24. https://doi.org/10.1016/j.jenvrad.2016.01.008

8. Campayo L, Grandjean A, Coulon A, et al (2011) Incorporation of iodates into hydroxyapatites: a new approach for the confinement of radioactive iodine. Journal of Materials Chemistry 21:17609. https://doi.org/10.1039/c1jm14157k

9. Campayo L, Le Gallet S, Perret D, et al (2015) Relevance of the choice of spark plasma sintering parameters in obtaining a suitable microstructure for iodine-bearing apatite designed for the conditioning of I-129. Journal of Nuclear Materials 457:63–71. https://doi.org/10.1016/j.jnucmat.2014.10.026

10. Lemesle T, Méar FO, Campayo L, et al (2014) Immobilization of radioactive iodine in silver aluminophosphate glasses. Journal of Hazardous Materials 264:117–126. https://doi.org/10.1016/j.jhazmat.2013.11.019

11. Laurencin D, Vantelon D, Briois V, et al (2014) Investigation of the local environment of iodate in hydroxyapatite by combination of X-ray absorption spectroscopy and DFT modeling. Royal Society of Chemistry Advances 4:14700–14707. https://doi.org/10.1039/C3RA47691J

12. Riley BJ, Vienna JD, Strachan DM, et al (2016) Materials and processes for the effective capture and immobilization of radioiodine: A review. Journal of Nuclear Materials 470:307–326. https://doi.org/10.1016/j.jnucmat.2015.11.038

13. Chong S, Peterson JA, Riley BJ, et al (2018) Glass-bonded iodosodalite waste form for immobilization of ^{129}I. Journal of Nuclear Materials 504:109–121. https://doi.org/10.1016/j.jnucmat.2018.03.033

14. Chong S, Riley BJ, Asmussen RM, et al (2020) Iodosodalite synthesis with hot isostatic pressing of precursors produced from aqueous and hydrothermal processes. Journal of Nuclear Materials 538:152222. https://doi.org/10.1016/j.jnucmat.2020.152222

15. An H, Kweon S, Park S, et al (2020) Immobilization of radioiodine via an interzeolite transformation to iodosodalite. Nanomaterials 10:2157. https://doi.org/10.3390/nano10112157

16. Moore RC, Pearce CI, Morad JW, et al (2020) Iodine immobilization by materials through sorption and redox-driven processes: A literature review. Science of The Total Environment 716:132820. https://doi.org/10.1016/j.scitotenv.2019.06.166

17. Pénélope R, Campayo L, Fournier M, et al (2022) Solid sorbents for gaseous iodine capture and their conversion into stable waste forms. Journal of Nuclear Materials 563:153635. https://doi.org/10.1016/j.jnucmat.2022.153635

18. Chabauty A-L, Campayo L, Méar FO, Montagne L (2019) Niobium- and bismuth-silver phosphate glasses for the conditioning of radioactive iodine. Journal of Non-Crystalline Solids 510:51–61. https://doi.org/10.1016/j.jnoncrysol.2019.01.015

19. Chabauty A-L, Méar FO, Montagne L, Campayo L (2021) Chemical durability evaluation of silver phosphate–based glasses designed for the conditioning of radioactive iodine. Journal of Nuclear Materials 550:152919. https://doi.org/10.1016/j.jnucmat.2021.152919

20. Du L-S, Stebbins JF (2005) Network connectivity in aluminoborosilicate glasses: A high-resolution ^{11}B, ^{27}Al and ^{17}O NMR study. Journal of Non-Crystalline Solids 351:3508–3520. https://doi.org/10.1016/j.jnoncrysol.2005.08.033

21. Holland D, Parkinson BG, Islam MM, et al (2007) NMR insights into wasteforms for the vitrification of high-level nuclear waste. Applied Magnetic Resonance 32:483–497. https://doi.org/10.1007/s00723-007-0038-8

22. Collin M, Fournier M, Frugier P, et al (2018) Structure of International Simple Glass and properties of passivating layer formed in circumneutral pH conditions. Nature Materials Degradation 2:4. https://doi.org/10.1038/s41529-017-0025-y

23. Angeli F, Charpentier T, Jollivet P, et al (2018) Effect of thermally induced structural disorder on the chemical durability of International Simple Glass. Nature Materials Degradation 2:31. https://doi.org/10.1038/s41529-018-0052-3

24. Charpentier T, Martel L, Mir AH, et al (2016) Self-healing capacity of nuclear glass observed by NMR spectroscopy. Scientific Reports 6:25499. https://doi.org/10.1038/srep25499

25. Riley BJ, Schweiger MJ, Kim D-S, et al (2014) Iodine solubility in a low-activity waste borosilicate glass at 1000°C. Journal of Nuclear Materials 452:178–188. https://doi.org/10.1016/j.jnucmat.2014.04.027

26. Muller IS, McKeown DA, Pegg IL (2014) Structural behavior of Tc and I ions in nuclear waste glass. Procedia Materials Science 7:53–59. https://doi.org/10.1016/j.mspro.2014.10.008

27. McKeown DA, Muller IS, Pegg IL (2015) Iodine valence and local environments in borosilicate waste glasses using X-ray absorption spectroscopy. Journal of Nuclear Materials 456:182–191. https://doi.org/10.1016/j.jnucmat.2014.09.033

28. Cicconi MR, Pili E, Grousset L, et al (2019) Iodine solubility and speciation in glasses. Scientific Reports 9:7758. https://doi.org/10.1038/s41598-019-44274-4

29. Cicconi MR, Pili E, Grousset L, Neuville DR (2019) The influence of glass composition on iodine solubility. MRS Advances 4:971–979. https://doi.org/10.1557/adv.2018.665

30. Jolivet V, Morizet Y, Paris M, Suzuki-Muresan T (2020) High pressure experimental study on iodine solution mechanisms in nuclear waste glasses. Journal of Nuclear Materials 533:152112. https://doi.org/10.1016/j.jnucmat.2020.152112

31. Gin S, Abdelouas A, Criscenti LJ, et al (2013) An international initiative on long-term behavior of high-level nuclear waste glass. Materials Today 16:243–248. https://doi.org/10.1016/j.mattod.2013.06.008

32. Piepel GF, Cooley SK, Vienna JD, Crum JV (2015) Experimental design for Hanford low-activity waste glasses with high waste loading. US Department of Energy, Pacific Northwest National Laboratory 24391.

33. Morizet Y, Hamon J, La C, et al (2021) Immobilization of ^{129}I in nuclear waste glass matrixes synthesized under high-pressure conditions: an experimental study. Journal of Materials Chemistry A 9:23902–23915. https://doi.org/10.1039/D1TA05011G

34. Bureau H, Auzende A-L, Marocchi M, et al (2016) Modern and past volcanic degassing of iodine. Geochimica et Cosmochimica Acta 173:114–125. https://doi.org/10.1016/j.gca.2015.10.017

35. Leroy C, Bureau H, Sanloup C, et al (2019) Xenon and iodine behaviour in magmas. Earth and Planetary Science Letters 522:144–154. https://doi.org/10.1016/j.epsl.2019.06.031

36. Vénague B, Campayo L, Toplis MJ, et al (2022) Role of alkalis on the incorporation of iodine in simple borosilicate glasses. Journal of Non-Crystalline Solids 576:121278. https://doi.org/10.1016/j.jnoncrysol.2021.121278

37. Morizet Y, Jolivet V, Trcera N, et al (2021) Iodine local environment in high pressure borosilicate glasses: An X-ray photoelectron spectroscopy and X-ray absorption spectroscopy investigation. Journal of Nuclear Materials 553:153050. https://doi.org/10.1016/j.jnucmat.2021.153050

38. Neeway J, Abdelouas A, Grambow B, et al (2012) Vapor hydration of SON68 glass from 90°C to 200°C: A kinetic study and corrosion products investigation. Journal of Non-Crystalline Solids 358:2894–2905. https://doi.org/10.1016/j.jnoncrysol.2012.07.020

39. Jolivet V, Jossé L, Rivoal M, et al (2019) Quantification of boron in aluminoborosilicate glasses using Raman and ^{11}B NMR. Journal of Non-Crystalline Solids 511:50–61. https://doi.org/10.1016/j.jnoncrysol.2018.12.038

40. Portier J, Campet G, Etourneau J, Tanguy B (1994) A simple model for the estimation of electronegativities of cations in different electronic states and coordinations. Journal of Alloys and Compounds 209:285–289. https://doi.org/10.1016/0925-8388(94)91115-0

41. Portier J, Campet G, Etourneau J, et al (1994) A simple approach to materials design: role played by an ionic-covalent parameter based on polarizing power and electronegativity. Journal of Alloys and Compounds 209:59–64. https://doi.org/10.1016/0925-8388(94)91076-6

42. Morizet Y, Brooker RA, Kohn SC (2002) CO_2 in haplo-phonolite melt: solubility, speciation and carbonate complexation. Geochimica et Cosmochimica Acta 66:1809–1820. https://doi.org/10.1016/S0016-7037(01)00893-6

43. Ojovan MI (2016) Mass spectrometric evidencing on modified random network microstructure and medium range order in silicate glasses. Journal of Non-Crystalline Solids 434:71–78. https://doi.org/10.1016/j.jnoncrysol.2015.12.015

44. Jolivet V, Morizet Y, Hamon J, et al (2021) The influence of iodide on glass transition temperature of high-pressure nuclear waste glasses. Journal of American Ceramic Society 104:1360–1369. https://doi.org/10.1111/jace.17571

45. Tougaard S (1997) Universality classes of inelastic electron scattering cross-sections. Surface and Interface Analysis 25:137–154. https://doi.org/10.1002/(SICI)1096-9918(199703)25:3<137::AID-SIA230>3.0.CO;2-L

46. Larre C, Morizet Y, Bézos A, et al (2020) Particular H_2O dissolution mechanism in iron-rich melt: Application to martian basaltic melt genesis. Journal of Raman Spectroscopy 51:493–507. https://doi.org/10.1002/jrs.5787

47. Tojo S, Tachikawa T, Fujitsuka M, Majima T (2008) Iodine-doped TiO_2 photocatalysts: correlation between band structure and mechanism. Journal of Physical Chemistry C 112:14948–14954. https://doi.org/10.1021/jp804985f

48. Marinoiu A, Gatto I, Raceanu M, et al (2017) Low cost iodine doped graphene for fuel cell electrodes. International Journal of Hydrogen Energy 42:26877–26888. https://doi.org/10.1016/j.ijhydene.2017.07.036

49. Moulder JF, Stickle WF, Sobol PE, Bomben KD (1992) Handbook of X-ray Photoelectron Spectroscopy: a reference book of standard spectra for identification and interpretation of XPS spectra. J Chastain Ed., Perkin-Elmer Corporation Physical Electronics Division, Eden Prairie, Minnesota.

50. Duffy JA (1986) The refractivity and optical basicity of glass. Journal of Non-Crystalline Solids 86:149–160. https://doi.org/10.1016/0022-3093(86)90484-9

51. Duffy JA (1989) A common optical basicity scale for oxide and fluoride glasses. Journal of Non-Crystalline Solids 109:35–39. https://doi.org/10.1016/0022-3093(89)90438-9

52. Duffy JA (2002) The electronic polarisability of oxygen in glass and the effect of composition. Journal of Non-Crystalline Solids 297:275–284. https://doi.org/10.1016/S0022-3093(01)00940-1

53. Duffy JA (2004) Relationship between optical basicity and thermochemistry of silicates. Journal of Physical Chemistry B 108:7641–7645. https://doi.org/10.1021/jp031209c

54. Duffy JA (2006) Ionic−Covalent character of metal and non metal oxides. Journal of Physical Chemistry A 110:13245–13248. https://doi.org/10.1021/jp063846j

55. Rodriguez CP, McCloy JS, Schweiger MJ, et al (2011) Optical basicity and nepheline crystallization in high alumina glasses. US Department of Energy, Pacific Northwest National Laboratory, 20184.

56. Dimitrov V, Komatsu T (1999) Electronic polarizability, optical basicity and non-linear optical properties of oxide glasses. Journal of Non-Crystalline Solids 249:160–179. https://doi.org/10.1016/S0022-3093(99)00317-8

57. Komatsu T, Dimitrov V, Tasheva T, Honma T (2021) Electronic polarizability in silicate glasses by comparison of experimental and theoretical optical basicities. International Journal of Applied Glass Science 12:424–442. https://doi.org/10.1111/ijag.16009

58. Dimitrov V, Sakka S (1996) Electronic oxide polarizability and optical basicity of simple oxides. I. Journal of Applied Physics 79:1736–1740. https://doi.org/10.1063/1.360962

59. Allred AL, Rochow EG (1958) A scale of electronegativity based on electrostatic force. Journal of Inorganic and Nuclear Chemistry 5:264–268. https://doi.org/10.1016/0022-1902(58)80003-2

60. Dimitrov V, Komatsu T, Tasheva T (2018) Group optical basicity and single bond strength of oxide glasses. Journal of Chemical Technology and Metallurgy 53:1038-1046.

61. Martens R, Müller-Warmuth W (2000) Structural groups and their mixing in borosilicate glasses of various compositions – an NMR study. Journal of Non-Crystalline Solids 265:167–175. https://doi.org/10.1016/S0022-3093(99)00693-6

62. Angeli F, Charpentier T, De Ligny D, Cailleteau C (2010) Boron speciation in soda-lime borosilicate glasses containing zirconium: Boron speciation in soda-lime borosilicate glasses. Journal of the American Ceramic Society 93:2693–2704. https://doi.org/10.1111/j.1551-2916.2010.03771.x

63. Maekawa H, Nakao T, Shimokawa S, Yokokawa T (1997) Coordination of sodium ions in $NaAlO_2$-SiO_2 melts: a high temperature ^{23}Na NMR study. Physics and Chemistry of Minerals 24:53–65. https://doi.org/10.1007/s002690050017

64. Schneider J, Mastelaro VR, Zanotto ED, et al (2003) Q^n distribution in stoichiometric silicate glasses: thermodynamic calculations and ^{29}Si high resolution NMR measurements. Journal of Non-Crystalline Solids 325:164–178. https://doi.org/10.1016/S0022-3093(03)00332-6

65. Malfait WJ, Halter WE, Morizet Y, et al (2007) Structural control on bulk melt properties: Single and double quantum ^{29}Si NMR spectroscopy on alkali-silicate glasses. Geochimica et Cosmochimica Acta 71:6002–6018. https://doi.org/10.1016/j.gca.2007.09.011

66. Morizet Y, Paris M, Gaillard F, Scaillet B (2014) Carbon dioxide in silica-undersaturated melt Part II: Effect of CO_2 on quenched glass structure. Geochimica et Cosmochimica Acta 144:202–216. https://doi.org/10.1016/j.gca.2014.08.034

67. Stebbins JF, Kroeker S, Lee SK, Kiczenski TJ (2000) Quantification of five- and six-coordinated aluminum ions in aluminosilicate and fluoride-containing glasses by high-field, high-resolution ^{27}Al NMR. Journal of Non-Crystalline Solids 275:1-6.

68. Allwardt JR, Stebbins JF, Terasaki H, et al (2007) Effect of structural transitions on properties of high-pressure silicate melts: ^{27}Al NMR, glass densities, and melt viscosities. American Mineralogist 92:1093–1104. https://doi.org/10.2138/am.2007.2530

69. Morizet Y, Vuilleumier R, Paris M (2015) A NMR and molecular dynamics study of CO_2-bearing basaltic melts and glasses. Chemical Geology 418:89–103. https://doi.org/10.1016/j.chemgeo.2015.03.021

70. Kuryaeva RG (2009) Effect of pressure on the refractive index and relative density of the $CaO{\cdot}Al_2O_3{\cdot}6SiO_2$ glass. Journal of Non-Crystalline Solids 355:159–163. https://doi.org/10.1016/j.jnoncrysol.2008.11.020

71. Komatsu T, Dimitrov V, Tasheva T, Honma T (2020) A review: A new insight for electronic polarizability and chemical bond strength in Bi_2O_3-based glasses. Journal of Non-Crystalline Solids 550:120365. https://doi.org/10.1016/j.jnoncrysol.2020.120365

72. Lebouteiller A, Courtine P (1998) Improvement of a bulk optical basicity table for oxidic systems. Journal of Solid State Chemistry 137:94–103. https://doi.org/10.1006/jssc.1997.7722

73. Bordes-Richard E, Courtine P (2005) Optical basicity: A scale of acidity/basicity of solids and its application to oxidation catalysis. In: Fierro J (ed) Metal Oxides. CRC Press, pp 319–352

74. Reddy RR, Nazeer Ahammed Y, Abdul Azeem P, et al (2001) Electronic polarizability and optical basicity properties of oxide glasses through average electronegativity. Journal of Non-Crystalline Solids 286:169–180. https://doi.org/10.1016/S0022-3093(01)00481-1

75. Honma T, Sato R, Benino Y, et al (2000) Electronic polarizability, optical basicity and XPS spectra of Sb_2O_3–B_2O_3 glasses. Journal of Non-Crystalline Solids 272:1–13. https://doi.org/10.1016/S0022-3093(00)00156-3

76. Inoue T, Honma T, Dimitrov V, Komatsu T (2010) Approach to thermal properties and electronic polarizability from average single bond strength in ZnO-Bi_2O_3-B_2O_3 glasses. Journal of Solid State Chemistry 183:3078–3085. https://doi.org/10.1016/j.jssc.2010.10.027

77. R. Moretti (2009) Polymerisation, basicity, oxidation state and their role in ionic modelling of silicate melts. Annals of Geophysics 48:. https://doi.org/10.4401/ag-3221

78. Duffy JA (2011) Oxidic glasses as hosts for migrating metal ions. Journal of Solid State Electrochemistry 15:87–93. https://doi.org/10.1007/s10008-009-0980-5

79. Lu X, Deng L, Du J, Vienna JD (2021) Predicting boron coordination in multicomponent borate and borosilicate glasses using analytical models and machine learning. Journal of Non-Crystalline Solids 553:120490. https://doi.org/10.1016/j.jnoncrysol.2020.120490

80. Wondraczek L, Sen S, Behrens H, Youngman RE (2007) Structure-energy map of alkali borosilicate glasses: Effects of pressure and temperature. Physical Review B 76:014202. https://doi.org/10.1103/PhysRevB.76.014202

81. Lee SK (2010) Effect of pressure on structure of oxide glasses at high pressure: Insights from solid-state NMR of quadrupolar nuclides. Solid State Nuclear Magnetic Resonance 38:45–57. https://doi.org/10.1016/j.ssnmr.2010.10.002

82. Bista S, Stebbins JF, Wu J, Gross TM (2017) Structural changes in calcium aluminoborosilicate glasses recovered from pressures of 1.5 to 3 GPa: Interactions of two network species with coordination number increases. Journal of Non-Crystalline Solids 478:50–57. https://doi.org/10.1016/j.jnoncrysol.2017.09.053

83. Wang Z, Zhao Y, Zhang C (2020) Comparative investigation on the structure and physical properties of CeO_2/TiO_2/Sb_2O_3-doped bismuth borosilicate glasses. Journal of Non-Crystalline Solids 544:120190. https://doi.org/10.1016/j.jnoncrysol.2020.120190

84. Dimitrov V, Komatsu T (2013) Optical basicity and chemical bonding of Bi_2O_3 containing glasses. Journal of Non-Crystalline Solids 382:18–23. https://doi.org/10.1016/j.jnoncrysol.2013.10.005

85. Fang L, Liu H, Zhao D, et al (2014) Reducing the reaction between boron-containing sealing glass-ceramics and lanthanum-containing cathode: Effect of Bi_2O_3. Journal of the European Ceramic Society 34:4463–4468. https://doi.org/10.1016/j.jeurceramsoc.2014.07.006

86. Zhu X, Mai C, Li M (2014) Effects of B_2O_3 content variation on the Bi ions in Bi_2O_3–B_2O_3–SiO_2 glass structure. Journal of Non-Crystalline Solids 388:55–61. https://doi.org/10.1016/j.jnoncrysol.2013.12.007

87. Chutithanapanon N, Bootjomchai C, Laopaiboon R (2019) Investigation of the optical properties of borosilicate glass recycled from high-pressure sodium lamp glass: Compositional dependence by addition of Bi_2O_3. Journal of Physics and Chemistry of Solids 132:244–251. https://doi.org/10.1016/j.jpcs.2019.05.005

88. Yokokawa T, Kawamura K, Maekawa H, Sawaguchi N (1999) Equilibrium of $O^{2-} + O^0 = 2O^-$ in oxide melts -examinations of its reality by three approaches. Journal of Molecular Liquids 83:311-321.

89. Hung I, Gan Z, Gor'kov PL, et al (2016) Detection of "free" oxide ions in low-silica Ca/Mg silicate glasses: Results from $^{17}O \rightarrow {}^{29}Si$ HETCOR NMR. Journal of Non-Crystalline Solids 445–446:1–6. https://doi.org/10.1016/j.jnoncrysol.2016.04.042

90. Fincham CJB, Richardson FD (1954) The behaviour of sulphur in silicate and aluminate melts. Proceedings of the Royal Society of London. Series A, Mathematical and Physical Sciences 223:40-62.

Figure caption

Figure 1: I 3d XPS spectra obtained on I-bearing glasses for the alkali-bearing glass compositions with B_2O_3 > 10 mol.% (A): Na20B20Bi0, K20B20Bi0 and Rb20B20Bi0; and alkaline-earth-bearing glass compositions with B_2O_3 < 10 mol.% (B): Ca30B10Bi0, Sr30B10Bi0 and Ba30B10Bi0. The spectra are shown in the I $3d_{5/2}$ region for clarity. The determined iodine speciation is reported next to each spectrum. The entire set of spectra is available in the Suppl. Mat..

Figure 2: Change in the iodine solubility (in mol.%) as a function of glass composition expressed by the cation nature (alkali and alkaline-earth) and cation size ($Na^+ \rightarrow K^+ \rightarrow Rb^+$ and $Ca^{2+} \rightarrow Sr^{2+} \rightarrow Ba^{2+}$). The data points for the two investigated glass series are shown: B_2O_3 < 10 mol.% and B_2O_3 > 10 mol.%.

Figure 3: Change in Iono-Covalent Parameter (ICP_{Glass}) as a function of optical basicity (Λ_{Glass}) for iodine-free glasses reported in Table 1. The ICP_{Glass} values are calculated following the description of Portier et al. [40, 41], the Λ_{Glass} is calculated following the description of Duffy [50]. There is a negative correlation between ICP_{Glass} and Λ_{Glass} that is related to the overall electronic configuration of the glass composition.

Figure 4: Change in O 1s peak position as determined from the XPS spectra as a function of Λ_{Glass} for iodine-free glasses reported in Table 1. The negative correlation observed is consistent with the nature of the Λ_{Glass} that corresponds to the electron donor capacity of oxygen atoms within the glass. An error of ±0.1 eV is considered for the peak position and corresponds to the actual analytical error.

Figure 5: Iodine solubility (in mol.%) as a function of Λ_{Glass} (A) and ICP_{Glass} (B). The iodine solubility is positively correlated and negatively correlated to Λ_{Glass} and ICP_{Glass}, respectively. High Λ_{Glass} values represent a higher basic glass media able to share electrons from oxygen atoms and high ICP_{Glass} values represent a glass media with electronegative charges. These aspects are favoring the iodine dissolution as I^- species. I solubility data points from Jolivet et al. [30] and Morizet et al. [33] have also been added. We calculated the Λ_{Glass} for NH23-1 from Jolivet et al. [30] using $N_4 = 0$ and $N_4 = 0.45$ so as to show the impact of N_4 value on the Λ_{Glass}.

Figure 6: Change in iodine solubility as a function of K_{Oxygen} for the different studied glass series. The K_{Oxygen} has been calculated with the equation of Moretti [77] that relates the K_{Oxygen} to the element moderating parameters (γ_i). The increase in K_{Oxygen} denotes the increase in the free oxygen concentration according to Eq. 6. Several glass series: alkali with and without Bi_2O_3 and mixed alkali – alkaline-earth cation; have been fitted with an exponential function of the form $y = y_0 + A \times \exp(x / t)$; however, these trends remain hypothetical.

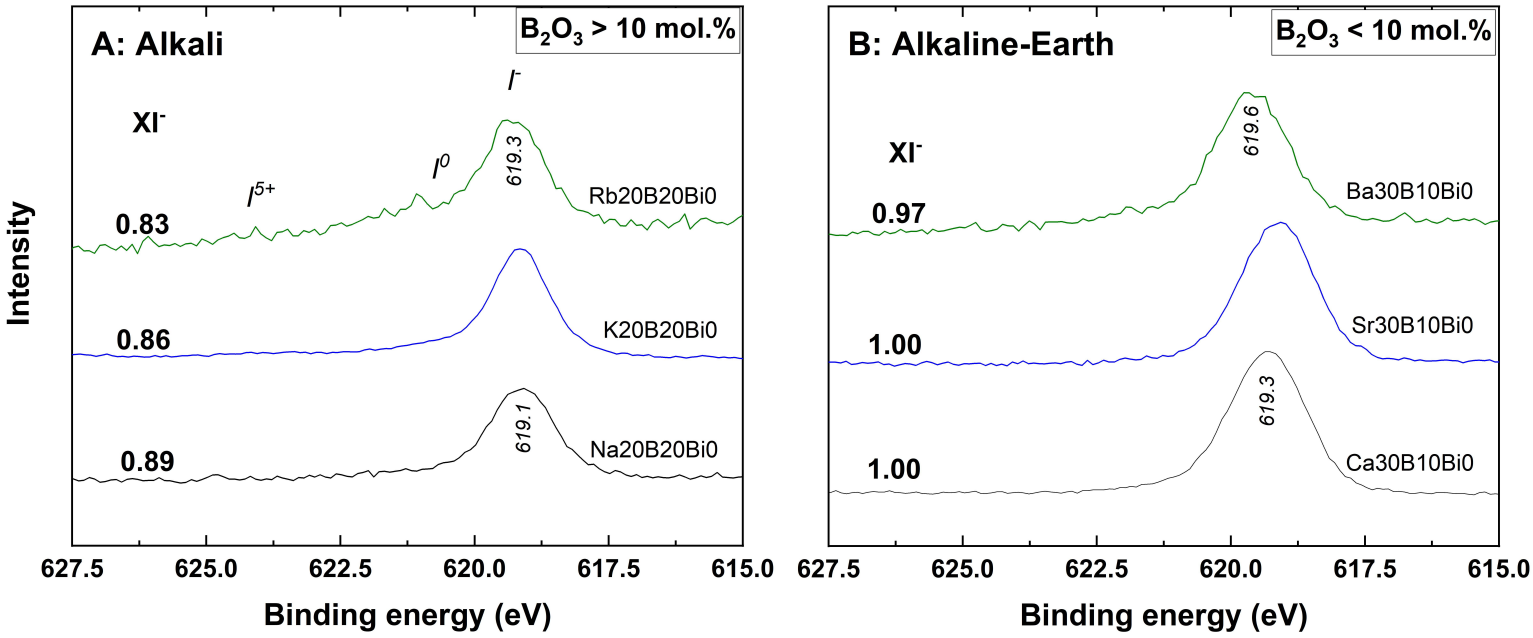
A: Alkali
B_2O_3 > 10 mol.%
I^-
XI-
I^{5+}
I^0
619.3
Rb20B20Bi0
0.83
K20B20Bi0
0.86
619.1
Na20B20Bi0
0.89
Intensity
627.5
625.0
622.5
620.0
617.5
615.0
Binding energy (eV)
B: Alkaline-Earth
B_2O_3 < 10 mol.%
XI-
619.6
Ba30B10Bi0
0.97
Sr30B10Bi0
1.00
619.3
Ca30B10Bi0
1.00
627.5
625.0
622.5
620.0
617.5
615.0
Binding energy (eV)

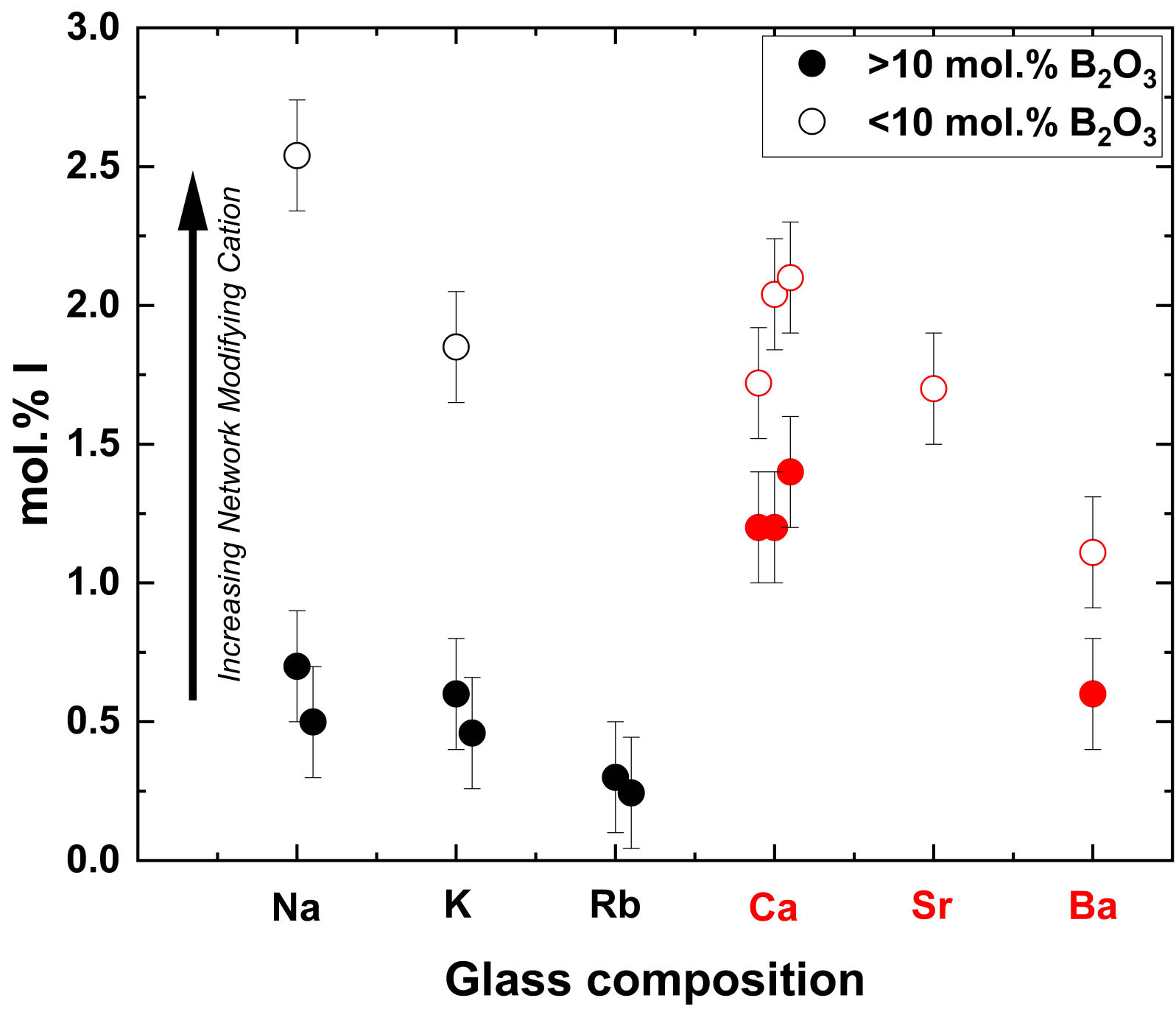
3.0
2.5
2.0
1.5
1.0
0.5
0.0
mol.% I
Increasing Network Modifying Cation
>10 mol.% B2O3
<10 mol.% B2O3
Na
K
Rb
Ca
Sr
Ba
Glass composition

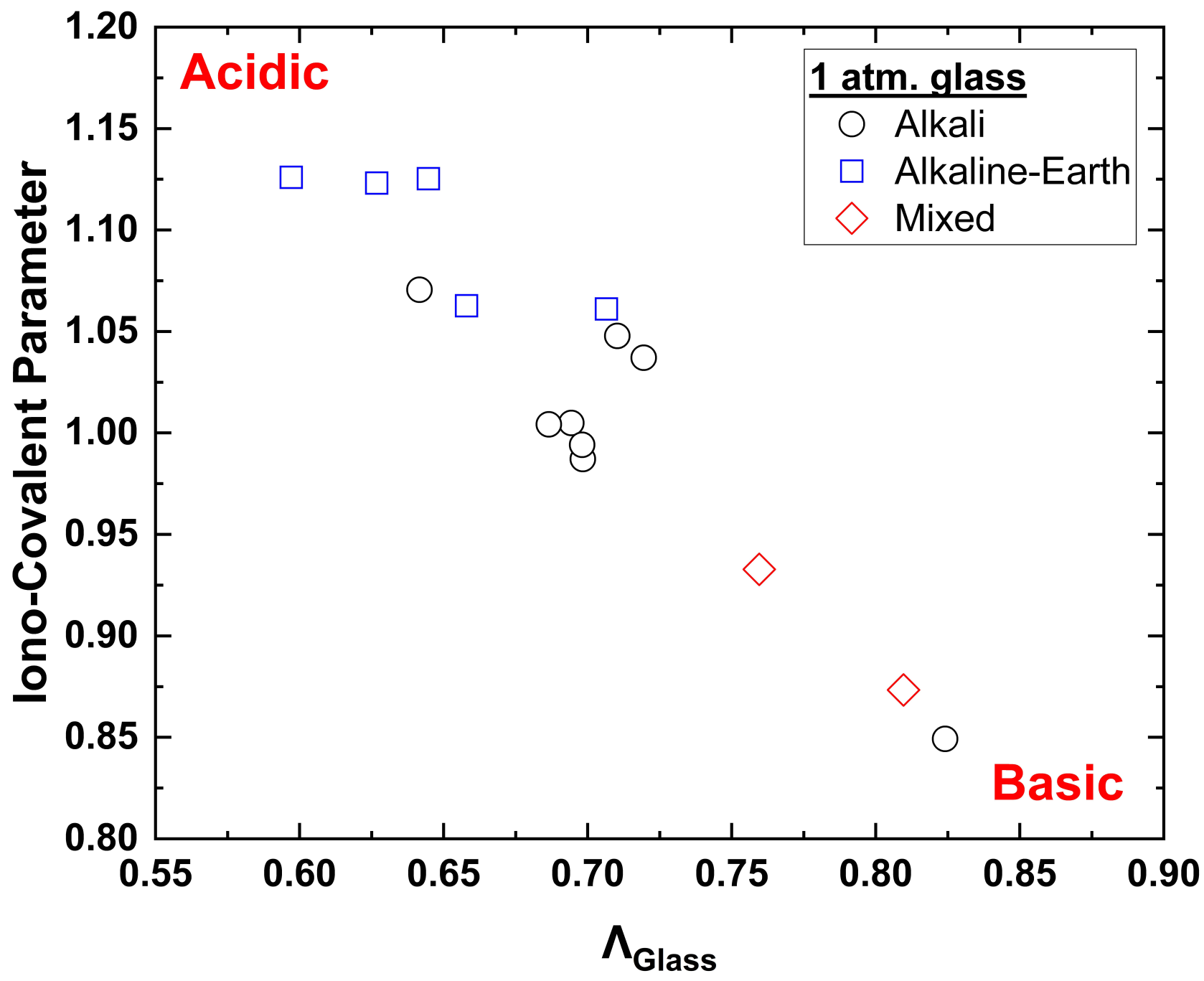
Acidic
Basic
1 atm. glass
Alkali
Alkaline-Earth
Mixed
Iono-Covalent Parameter
1.20
1.15
1.10
1.05
1.00
0.95
0.90
0.85
0.80
0.55
0.60
0.65
0.70
0.75
0.80
0.85
0.90
Λ Glass

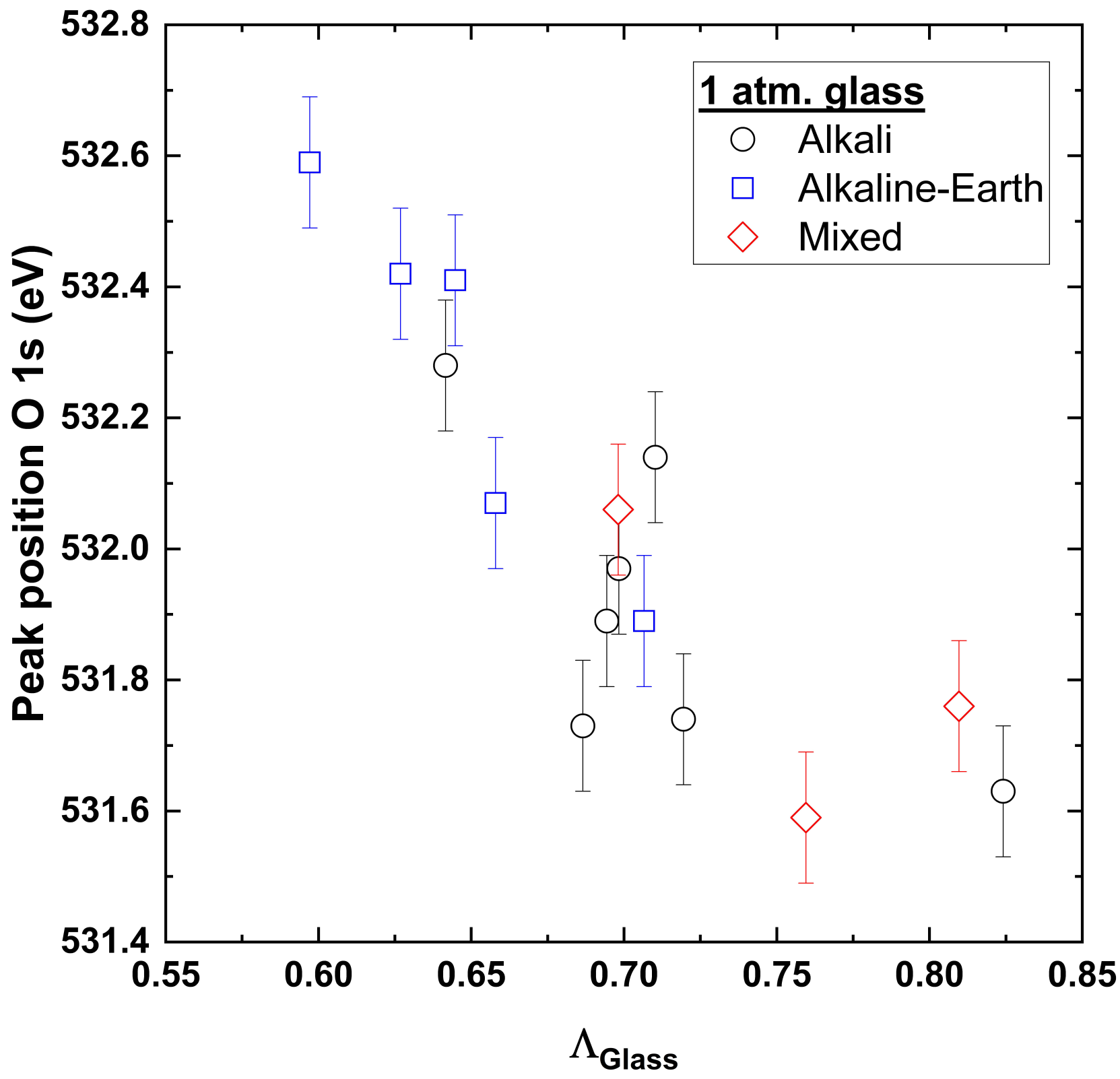
1 atm. glass
Alkali
Alkaline-Earth
Mixed
Peak position O 1s (eV)
532.8
532.6
532.4
532.2
532.0
531.8
531.6
531.4
0.55
0.60
0.65
0.70
0.75
0.80
0.85
Λ_{Glass}

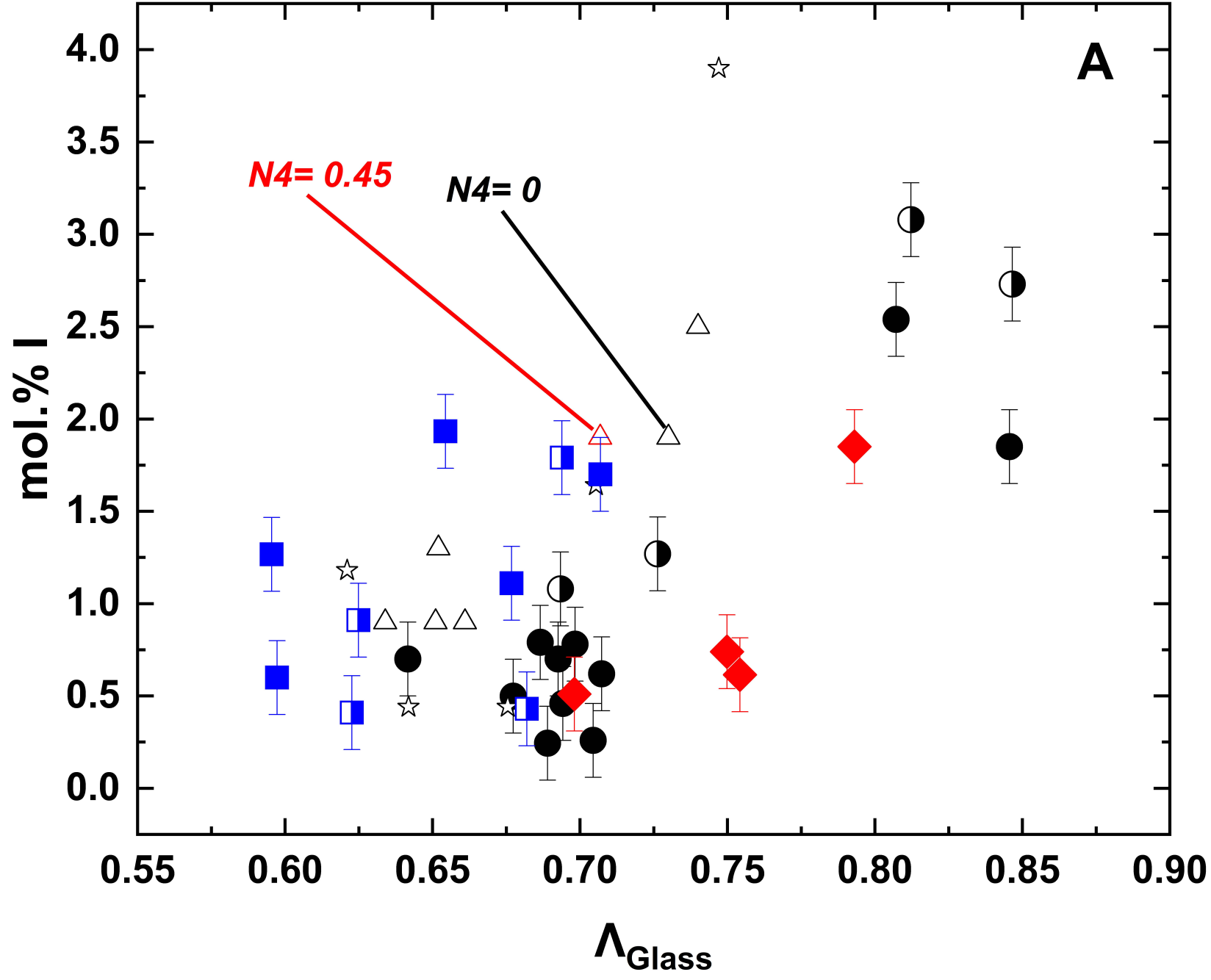
A
N4= 0.45
N4= 0
mol.% I
4.0
3.5
3.0
2.5
2.0
1.5
1.0
0.5
0.0
0.55
0.60
0.65
0.70
0.75
0.80
0.85
0.90
Λ Glass

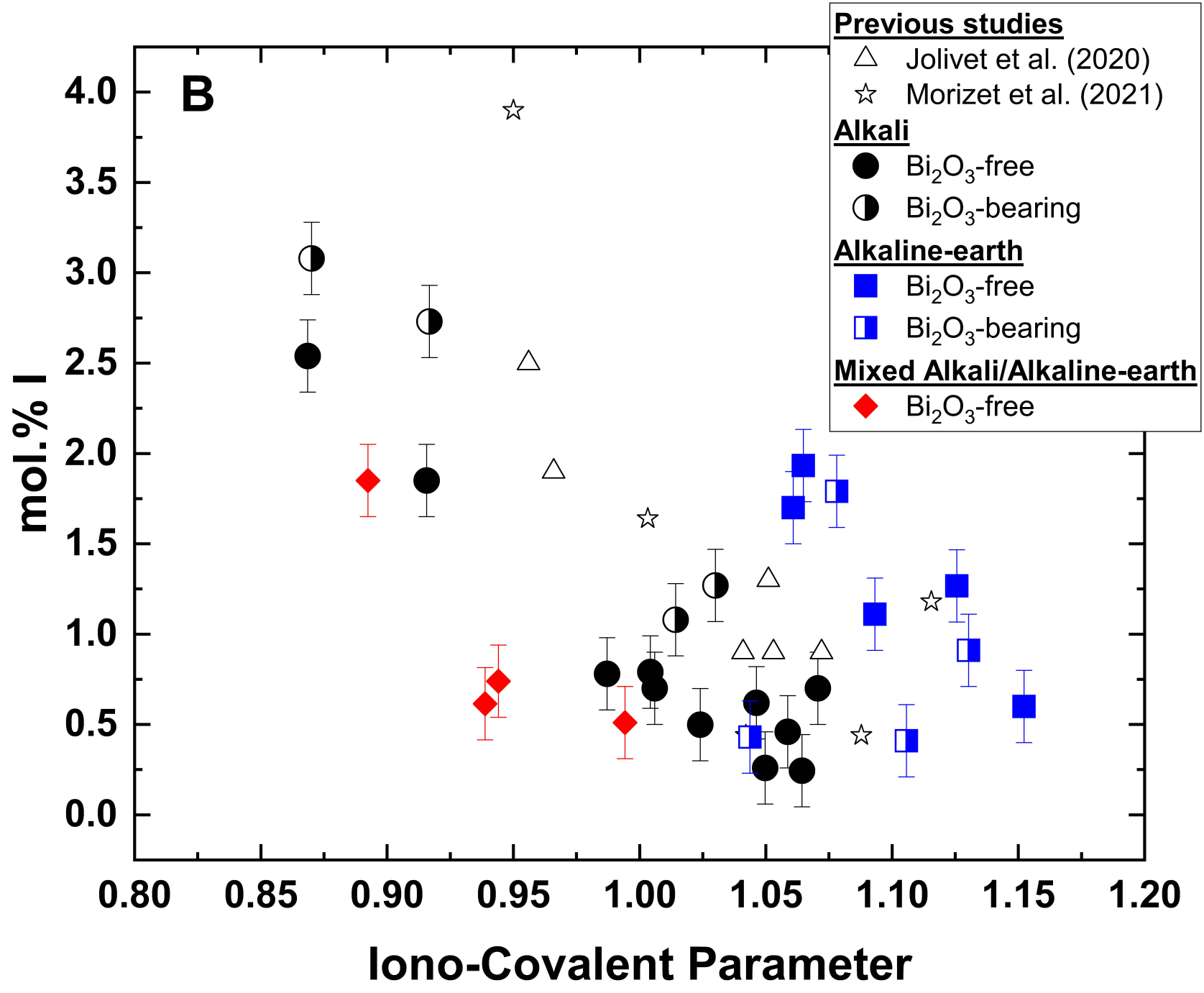
B
Previous studies
Jolivet et al. (2020)
Morizet et al. (2021)
Alkali
Bi2O3-free
Bi2O3-bearing
Alkaline-earth
Bi2O3-free
Bi2O3-bearing
Mixed Alkali/Alkaline-earth
Bi2O3-free
mol.% I
4.0
3.5
3.0
2.5
2.0
1.5
1.0
0.5
0.0
0.80
0.85
0.90
0.95
1.00
1.05
1.10
1.15
1.20
Iono-Covalent Parameter

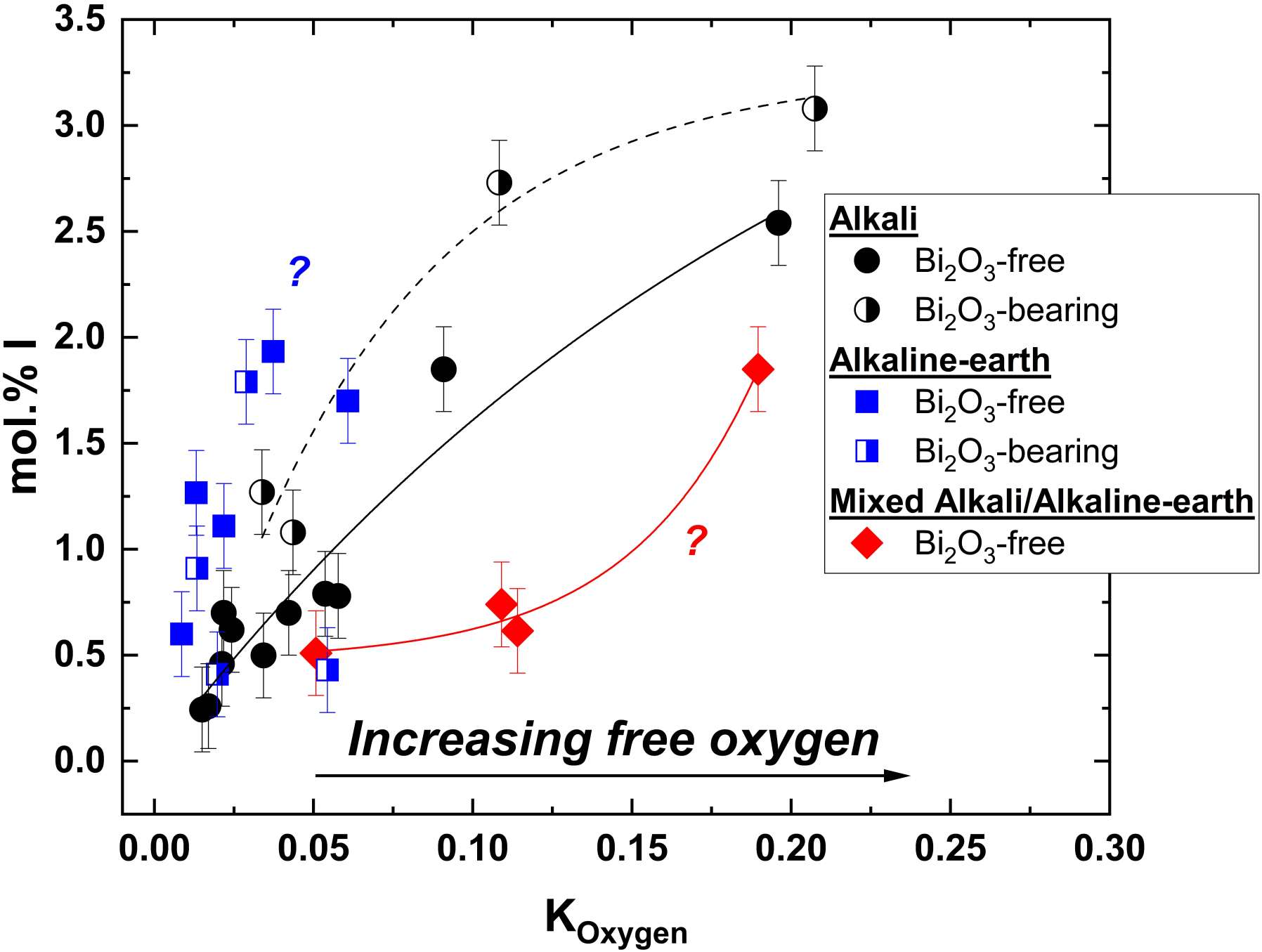
mol.% I
3.5
3.0
2.5
2.0
1.5
1.0
0.5
0.0
0.00
0.05
0.10
0.15
0.20
0.25
0.30
K Oxygen
?
?
Increasing free oxygen
Alkali
Bi2O3-free
Bi2O3-bearing
Alkaline-earth
Bi2O3-free
Bi2O3-bearing
Mixed Alkali/Alkaline-earth
Bi2O3-free